Exploring Stable Meta-optimization Patterns via Differentiable Reinforcement Learning for Few-shot Classification

Anonymous Authors

ABSTRACT

Existing few-shot learning methods generally focus on designing exquisite structures of meta-learners for learning task-specific prior to improve the discriminative ability of global embeddings. However, they often ignore the importance of learning stability in meta-training, making it difficult to obtain a relatively optimal model. From this key observation, we propose an innovative generic differentiable Reinforcement Learning (RL) strategy for few-shot classification. It aims to explore stable meta-optimization patterns in meta-training by learning generalizable optimizations for producing task-adaptive embeddings. Accordingly, our differentiable RL strategy models the embedding procedure of feature transformation layers in meta-learner to optimize the gradient flow implicitly. Also, we propose a memory module to associate historical and current task states and actions for exploring inter-task similarity. Notably, our RL-based strategy can be easily extended to various backbones. In addition, we propose a novel task state encoder to encode task representation, which fully explores inner-task similarities between support set and query set. Extensive experiments verify that our approach can improve the performance of different backbones and achieve promising results against state-of-the-art methods in few-shot classification. Our code is available at an anonymous site: https://anonymous.4open.science/r/db8f0c012/.

CCS CONCEPTS

• **Computing methodologies → Image representations**.

KEYWORDS

few-shot classification, differentiable reinforcement learning, stable meta-optimization.

1 INTRODUCTION

Few-shot learning [1, 18, 30, 42, 55] aims to explore generalizable visual knowledge from seen classes in training and then utilize the learned knowledge to correctly recognize unseen classes where only a few labeled samples are available. Few-shot learning has attracted ever-increasing interest in industrial and academic communities due to its various applications.

Generally, existing methods [20, 28, 32, 53] often rely on designing exquisite structures of meta-learner for generating discriminative global embeddings of images to achieve promising performance. Recently, exploring task-specific prior for meta-tasks has been proven as an efficient way to generate discriminative global embeddings. To this end, existing methods [5, 36, 55] usually adopt task-adapting strategies to model the task-specific prior. Ye *et al.* [55] modeled the task-adapting strategy as non-linear transformations on the support set. Qiao *et al.* [36] formulated the task-adapting process as a quadratic programming problem on sample-wise distance constraints. Baik *et al.* [5] proposed to implicitly guide the embedding procedure via optimizations of task-specific loss functions. Despite the improvement of these methods, the meta-training process still suffers from severe problems, such as high variance [4] and noisy gradients [43]. These problems can lead to unstable optimization patterns in meta-training and cause wrong optimization direction, finally affecting the performance, as illustrated in Figure 1(a).

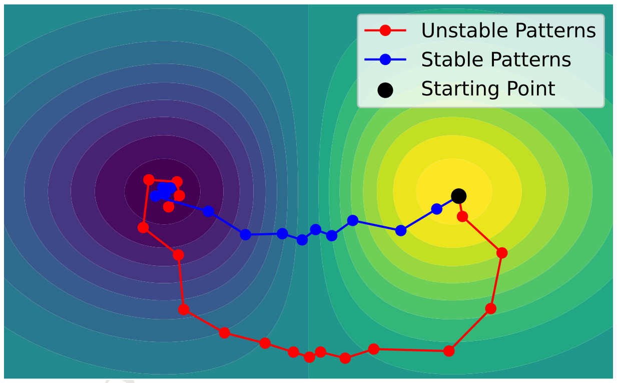

(a) An example of unstable optimization patterns.

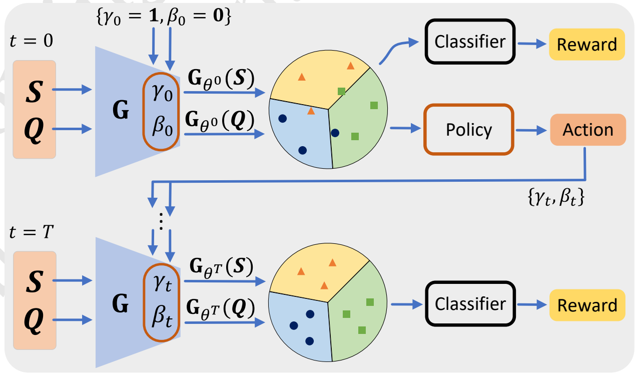

(b) Overview of our approach.

Figure 1: (a) The illustration of our motivation. Unstable patterns of meta-learner can lead to wrong optimization direction, causing extra gradient descent computation. (b) Overview of our differentiable RL strategy for modeling generalizable patterns of producing transformation layer parameters.

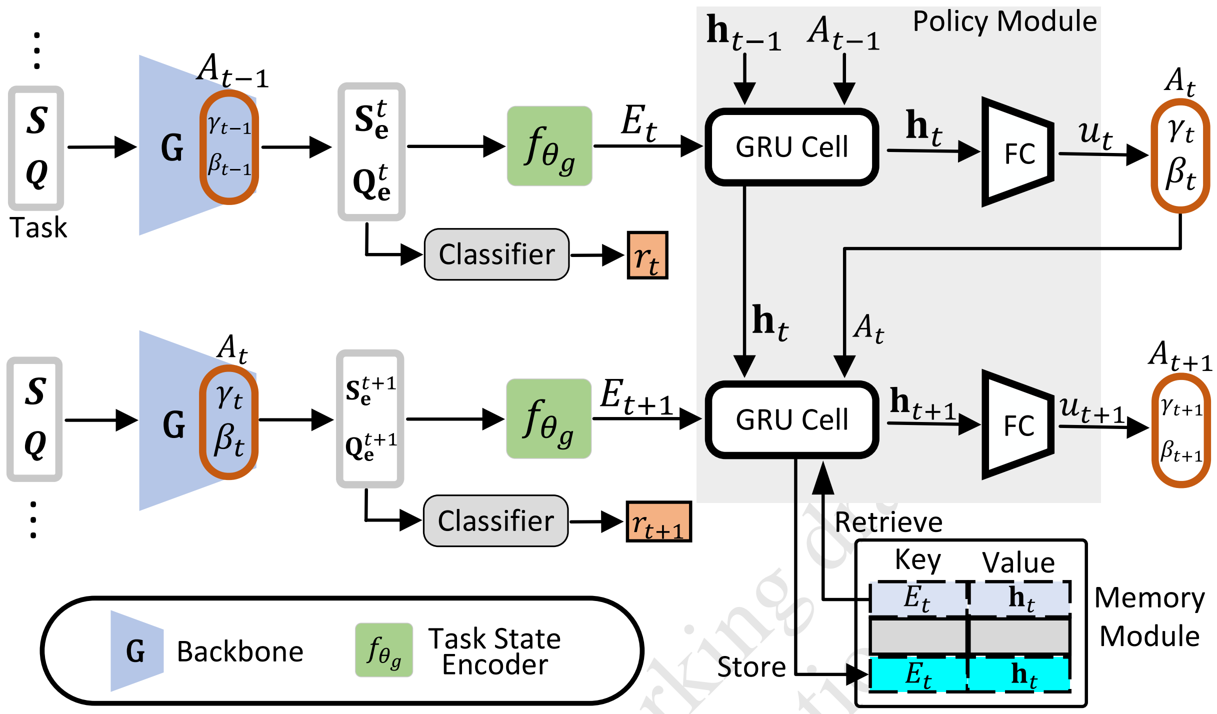

Figure 2: The details of our approach. We describe the transaction from time step t to $t+1$. The policy module, consisting of a GRU cell with a FC layer, takes the state of the current time step t as input and outputs the parameters of the transformation layer (*i.e.*, scale γ and shift β) as action A_t. The state of the current time step t is the concatenation of the current task state E_t and previous action A_{t-1}. The memory module enables rapid storage and retrieval of associations between task state E_t and hidden state h_t of action A_t.

Prior approaches of reinforcement learning, including training sample augment [9] and spatial attention enhancement [17], have proven their effectiveness in improving the performance of few-shot learning tasks. However, these methods mainly straightforwardly utilize RL in the pre-training stage, and they often suffer from unstable training and huge computational cost. This is because they model the environment as a non-differentiable black box, resulting in the training process requiring lots of trials and errors. Moreover, black-box RL is prone to underfit on unseen tasks outside of distribution [29]. For the meta-training stability, Anantha *et al.* [3] modeled the meta-learner as the agent of RL to learn the task-adaptive loss surface of base-learner for exploiting stable loss patterns. However, Anantha *et al.* [3] aims to stabilize the inner loop. In contrast, their approach is still limited to the outer loop since the environment lacks differentiability. Applying RL with a differentiable environment is proven to be efficient in robotics [29], control [14], and navigation [10], by the ability to stabilize optimization process and improve generalization on unseen tasks. This inspires us to utilize the pros of differentiable RL to overcome the flaws of black-box RL-based approaches (*e.g.*, optimization instability, and huge computational cost) in few-shot learning.

Highly inspired by differentiable RL [14, 29], we propose a generic differentiable RL-based meta-optimization strategy for few-shot classification (named **R**einforced **M**eta-**O**ptimization, **RMO**), as shown in Figure 1(b). Our method aims to explore stable meta-optimization patterns in meta-training for improving the discriminative ability of task-adaptive embeddings. Hence, we design a differentiable RL policy to model the embedding procedure of transformation layers in meta-learner for implicitly optimizing the gradient flow. Specifically, we model the policy as a Gated Recurrent Unit (GRU) to learn generalizable optimization patterns across meta-tasks. To this end, we propose a memory module, modeled as a Differentiable Neural Dictionary (DND), to associate historical and current task states and actions for exploring inter-task similarity and boosting the learning of policy. In addition, we propose a novel task state encoder to encode task state for fully exploring inner-task similarity between supports and queries. We conduct experiments with various backbones and classifiers on three popular datasets. The results verify that our method can consistently improve the performance on different backbones and achieve promising results against state-of-the-art transductive methods in few-shot classification.

Overall, the contributions are summarized as follows:

(1) We propose a generic differentiable RL-based few-shot learning strategy to explore stable meta-optimization patterns for meta-training. Our approach can be easily extended to various backbones, including ConvNet, ResNet, WRN, and DenseNet.
(2) We propose a novel task state encoder to encode task representation, enabling information adaptation and fully exploring inner-task similarities between support set and query set.
(3) Extensive experiments verify that our approach consistently improves the performance on various backbones and achieves promising results against state-of-the-art transductive methods in few-shot classification.

2 RELATED WORK

2.1 Few-shot Classification

Meta-learning has been proven to be an effective way to address the few-shot classification problem [18, 24, 30, 57, 59]. These methods often train a meta-learner using diverse meta-tasks sampled from a task distribution to capture common patterns across the tasks. The design of a meta-learner can include learning task-adapted representations [24, 30, 55], exploring inner-task correlations [18, 36], and utilizing text-modal knowledge [32, 51]. Introducing transformation layers into the network has proven efficient in learning task-specific representations. These methods include feature map modulation [30, 46], non-linear adaptation [55], task-level projection [57], and learning task-specific loss functions [5]. While these methods always tend to design complicated structures of meta-learner [17], they ignore the importance of stable optimization patterns in meta-training. These methods often suffer from overfitting in meta-training and need careful parameter tuning [30].

2.2 Stable Optimization for Few-shot Learning

MAML [12] is a powerful algorithm introducing meta-learning into diverse problems, including few-shot classification. It aims to learn optimizations to adapt to unseen tasks with few available training samples. However, MAML-based methods suffer from some problems, including training instability [4], permutation sensitivity [54], and memorization overfitting [56]. Solutions for MAML's shortcomings have been well studied. Ye *et al.* [54] proposed to initialize the classification weights with one single weight vector to overcome the permutation sensitivity problem in few-shot classification. Simon *et al.* [43] proposed to scale the noisy gradients of meta-learner via low-rank approximation to stabilize the meta-training. However, these methods mainly focus on improving the generic meta-learning algorithms. In few-shot learning, the stable optimization patterns in meta-training need further studying.

2.3 Reinforced Few-shot Learning

Reinforcement Learning has been proven effective in addressing the few-shot learning problem. Chu *et al.* [9] proposed to utilize maximum-entropy RL to learn the cropping trajectories of training images. Hong *et al.* [17] proposed to utilize the RL strategy to optimize spatial attention of feature maps. However, these methods only utilized the RL strategy into the pre-training stage, and these methods are still limited by the shortcomings of RL (*e.g.* unstable training and huge computational cost). On training stability of few-shot learning, Anantha *et al.* [3] proposed to learn the scale of gradients of base-learner task-dependently via RL to explore stable loss patterns in meta-training. However, this work only studied the optimization stability of the inner loop in meta-training, and for the outer loop, this method is still limited by the shortcomings of RL since the environment is modeled as a black box.

3 METHOD

Our approach (as shown in Figure 2) mainly consists of a policy module, a memory module, and a task state encoder. We describe each module and the optimization strategy of our whole method in the following subsections.

Problem statement. In the meta-training phase, the model faces a set of tasks. Each task is represented as a N-way K-shot problem with N classes sampled from the seen class set $\mathbb{S}$ (*i.e.*, classes in training set) and K labeled samples per class, which composes the support set. Besides, M unlabeled samples are sampled per class as the query set. We denote the support set as $\mathrm{S} = \{\mathbf{x}_i, \mathbf{y}_i\}_{i=1}^{NK}$ and the query set as $\mathrm{Q} = \{\mathbf{x}_i\}_{i=NK+1}^{NK+NM}$ with the instance $\mathbf{x}_i$ and the label $\mathbf{y}_i \in \mathbb{S}$. In validation and evaluation, the N classes are sampled from the unseen class set $\mathbb{U}$ (*i.e.*, classes in the validation set and testing set). Note that $\mathbb{S} \cap \mathbb{U} = \emptyset$. The goal is to find an optimal function f that correctly classifies the test sample $\mathbf{x}_{test}$ via $\hat{\mathbf{y}}_{test} = f(\mathbf{x}_{test}; \mathrm{S}) \in \mathbb{U}$.

Model design. First, we describe how the Feature-wise Linear Modulation (FiLM) layer [33] transforms the feature map. The learnable parameters of a FiLM layer include scale γ and shift β, where $\gamma, \beta \in \mathbb{R}^c$. We split the backbone network $\mathbf{G}$ into two parts, where $\mathbf{G}_1$ is the unchanged part and $\mathbf{G}_2$ is the part where a FiLM layer is inserted after the last Batch Normalization (BN) layer in each convolution block. An intermediate feature map $\mathbf{e}'_\mathbf{x} = \mathbf{G}_1(\mathbf{x})$ of an input image $\mathbf{x}$ is first obtained. Denote $\mathbf{z} \in \mathbb{R}^{h*w*c}$ is the activation of $\mathbf{e}'_\mathbf{x}$ produced by the BN layer in $\mathbf{G}_2$. Then $\mathbf{z}$ is modulated as: $\hat{z}_{h,w,c} = \gamma_c * z_{h,w,c} + \beta_c$, where $\hat{z}_{h,w,c} \in \hat{\mathbf{z}}$, $z_{h,w,c} \in \mathbf{z}$, and c denotes the number of channels. This modulation is applied in each block of $\mathbf{G}_2$. At last, the part $\mathbf{G}_2$ outputs the embedding $\mathbf{e}_\mathbf{x} \in \mathbb{R}^d$ of input image $\mathbf{x}$, denoted as $\mathbf{e}_\mathbf{x} = \mathbf{G}_2(\mathbf{e}'_\mathbf{x}; \gamma, \beta)$. Denote $\theta_\mathbf{G}$ as the set of all learnable parameters of $\mathbf{G}$. Different from previous methods [30, 39], we model the learning process of parameters γ and β with differentiable RL to optimize the gradient flow of the meta-learner. We describe how we model this process with the key elements of differentiable RL in the following.

State. RL is an iterative process where the policy takes the current state as input and picks up an action in each time step. Denote $t = 1, \cdots, T$ as the current time step and T as the total number of time steps. The next state S_{t+1} is obtained from a differentiable transition function: $S_{t+1} = \Phi(S_t, A_t)$. We model the state S_t as the concatenation of current task state E_t and previous action A_{t-1}. We depict how we obtain the task state E_t via task state encoder in **Section 3.3. Task State Encoder**.

Action. In each time step, the policy outputs an action based on the current task state. We model the action A_t as the concatenation of parameters γ_t and β_t. Here γ_t and β_t denotes the values of γ and β in time step t, respectively. We depict how the action A_t is picked up in **Section 3.1. Policy Module**.

Reward. The environment rewards the quality of the action to guide the RL model. The reward r_t is calculated with a differentiable function: $r_t = \Psi(S_t, A_t)$. We model the current reward r_t as the classification loss calculated by the classifier. We depict how the reward r_t is calculated in **Section 3.4. Optimization Strategy**.

3.1 Policy Module

We model the policy module as a minimal gated unit [60], a variant of GRU with one single forget gate, to improve efficiency and reduce the number of parameters. In each time step t, the embeddings $\{\mathbf{e}^t_\mathbf{x}, \mathbf{x} \in \mathrm{S} \cup \mathrm{Q}\}$ are first transformed into the task state E_t, then concatenated with previous action A_{t-1} to form input state S_t. Define $\gamma_0 = \mathbf{1}$ and $\beta_0 = \mathbf{0}$, where $\mathbf{1}$ and $\mathbf{0}$ are two vectors filled with 1 and 0. The GRU cell takes S_t as input and outputs the action $A_t = \{\gamma_t, \beta_t\}$

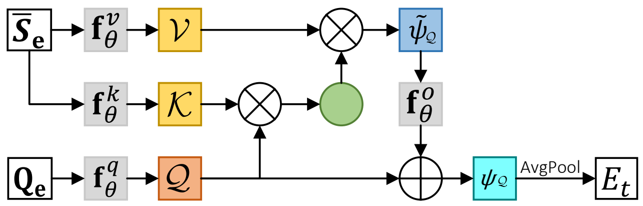

Figure 3: Overview of the task state encoder, which consists of a self-attention module followed by an average pooling layer.

via the following equations:

$$\begin{aligned}\mathbf{f}_t &= \sigma(\mathbf{W}_f \cdot [\mathbf{h}_{t-1}, S_t] + \mathbf{b}_f),\\ \tilde{\mathbf{h}}_t &= \tanh(\mathbf{W}_h \cdot [\mathbf{f}_t \odot \mathbf{h}_{t-1}, S_t] + \mathbf{b}_h),\\ \mathbf{h}_t &= (\mathbf{1} - \mathbf{f}_t) \odot \mathbf{h}_{t-1} + \mathbf{f}_t \odot \tilde{\mathbf{h}}_t,\end{aligned} \tag{1}$$

where $\sigma(\cdot)$ and $\tanh(\cdot)$ denote the sigmoid and hyperbolic tangent activation function, respectively, and $\odot$ denotes the Hadamard product. Then $\mathbf{h}_t$ is taken by a fully connected layer without bias to get the mean μ_t: $\mu_t = \mathbf{W}_u \cdot \mathbf{h}_t$. The action A_t is sampled from the normal distribution: $A_t \sim \mathcal{N}(\mu_t, 1)$. The value of $\mathbf{h}_0$ is initialized to $\mathbf{0}$ for each task.

3.2 Memory Module

Inspired by the idea of episodic control [34, 40], we model the memory module as a DND to explore inter-task similarity, enabling rapid storage and retrieve of associations between task state E_t and hidden state $\mathbf{h}_t$ of action A_t. The key and value of DND denote task state E_t and hidden state $\mathbf{h}_t$, respectively. Then the new $\mathbf{h}_t$ is calculated using the following equations:

$$\begin{aligned}\mathbf{f}_t &= \sigma(\mathbf{W}_f \cdot [\mathbf{h}_{t-1}, S_t] + \mathbf{b}_f),\\ \tilde{\mathbf{h}}_t &= \tanh(\mathbf{W}_h \cdot [\mathbf{f}_t \odot \mathbf{h}_{t-1}, S_t] + \mathbf{b}_h),\\ \mathbf{r}_t &= \tanh(\mathbf{W}_r \cdot [\mathbf{h}_{t-1}, S_t] + \mathbf{b}_r),\\ \mathbf{h}_t &= (\mathbf{1} - \mathbf{f}_t) \odot \mathbf{h}_{t-1} + \mathbf{f}_t \odot \tilde{\mathbf{h}}_t + \mathbf{r}_t \odot \tanh(\mathbf{h}_{ep}),\end{aligned} \tag{2}$$

where $\mathbf{h}_{ep}$ denotes the hidden state from DND: $\mathbf{h}_{ep} = DND\left[E_t'\right]$, and E_t' denotes the matched key of current E_t using a distance metric. We choose E_t' using top-1 cosine similarity with stored E_t: $d(E_t', E_t) = \frac{E_t' \cdot E_t}{\|E_t'\|\|E_t\|}$. Finally, $\mathbf{h}_t$ and E_t are stored to DND: $DND[E_t] = \mathbf{h}_t$. Denote θ_p as the set of all learnable parameters of policy module and D as the number of memory units in DND.

3.3 Task State Encoder

The architecture of the task state encoder is shown in Figure 3. Unlike previous methods [30, 39] that only consider inner-task information from the support set, we utilize a single-head self-attention module to explore inner-task similarities between support set and query set. Here, we omit time step t for simplicity. First, we obtain class representations by averaging the support samples in each class: $\bar{\mathbf{e}}_c = \frac{1}{K}\sum_{(\mathbf{x}_i,\mathbf{y}_i)\in \mathrm{S}_c} \mathbf{e}_{\mathbf{x}_i}$, where S_c denotes the support samples in c-th class, and $c = 1, \cdots, N$. Define $\bar{\mathrm{S}}_\mathrm{e} = \{\bar{\mathbf{e}}_c\}_{c=1}^N$ and $\mathrm{Q}_\mathrm{e} = \left\{\mathbf{e}_{\mathbf{x}_i}\right\}_{\mathbf{x}_i\in\mathrm{Q}}$. We construct the query, key, and value using the following equation:

$$\mathcal{Q} = \mathbf{f}_\theta^q(\mathrm{Q}_\mathrm{e}), \mathcal{K} = \mathbf{f}_\theta^k(\bar{\mathrm{S}}_\mathrm{e}), \mathcal{V} = \mathbf{f}_\theta^v(\bar{\mathrm{S}}_\mathrm{e}), \tag{3}$$

Algorithm 1 Training procedure of our approach.

```
Require: Seen class set $\mathbb{S}$, classifier $f_m$
 1: while training do
 2:     Sample $N$-way $K$-shot task $(\mathrm{S}, \mathrm{Q})$ from $\mathbb{S}$
 3:     Compute $\mathbf{e}_\mathbf{x}^0 = \mathrm{G}(\mathbf{x}; \gamma_0, \beta_0)$ for all $\mathbf{x} \in \mathrm{S} \cup \mathrm{Q}$
 4:     Compute $L_c$ for all $\mathbf{x}_{test} \in \mathrm{Q}$ with $f_m$
 5:     Reset $\mathbf{h}_0 = \mathbf{0}$
 6:     for all $t = 1, \cdots, T$ do
 7:         Compute $S_t = \{E_t, \gamma_{t-1}, \beta_{t-1}\}$ for all $\mathbf{e}_\mathbf{x}^{t-1}$
 8:         Compute $A_t = \{\gamma_t, \beta_t\}$ for $S_t$
 9:         Compute $\mathbf{e}_\mathbf{x}^t = \mathrm{G}(\mathbf{x}; \gamma_t, \beta_t)$ for all $\mathbf{x} \in \mathrm{S} \cup \mathrm{Q}$
10:         Compute $r_t$ for all $\mathbf{x}_{test} \in \mathrm{Q}$ with $f_m$
11:     end for
12:     Compute $L_r$ for all $\{r_t\}_{t=1}^T$
13:     Update parameters $\theta_\mathrm{G}$, $\theta_p$, and $\theta_g$ with $L_{total}$
14: end while
15: return Parameters $\theta_\mathrm{G}$, $\theta_p$, and $\theta_g$
```

where the support classes and query samples are mapped by three linear projections, $\mathbf{f}_\theta^q$, $\mathbf{f}_\theta^k$, and $\mathbf{f}_\theta^v$, respectively. The calculation of task state E is formulated as:

$$\begin{aligned}\tilde{\psi_Q} &= softmax(\frac{\mathcal{Q}\mathcal{K}^T}{\sqrt{d}})\mathcal{V},\\ \psi_Q &= \tau(\mathcal{Q} + \mathbf{f}_\theta^o(\tilde{\psi_Q})),\\ E &= AvgPool(\psi_Q),\end{aligned} \tag{4}$$

where $\mathbf{f}_\theta^o$ is a linear projection and τ denotes the sequence of dropout [45] and layer normalization [52]. Finally, E is calculated via the average pooling operation, denoted by $AvgPool(\cdot)$. Denote θ_g as the set of all learnable parameters of the task state encoder.

3.4 Training Strategy

We choose 3 popular classifiers: ProtoNet [44], DSN [42], and MetaOptNet [23]. The corresponding models are named RMO-PN, RMO-DSN, and RMO-MON, respectively. Denote the predicted probability distribution of test sample $(\mathbf{x}_q, \mathbf{y}_q)$ as $p(\hat{\mathbf{y}}_q = \mathbf{y}_q \mid \mathbf{e}_{\mathbf{x}_q}; f_m)$, where f_m denotes the classifier. We first define the classification loss as:

$$L_c = -\log p(\hat{\mathbf{y}}_q = \mathbf{y}_q \mid \mathrm{G}(\mathbf{x}_q; \gamma_0, \beta_0)). \tag{5}$$

Then, in each time step t, the log-probability is calculated as the reward:

$$r_t = \log p(\hat{\mathbf{y}}_q = \mathbf{y}_q \mid \mathrm{G}(\mathbf{x}_q; \gamma_t, \beta_t)). \tag{6}$$

The goal is to maximize the accumulated rewards $\{r_t\}_{t=1}^T$. Denote γ as the discount factor. We define the reinforcement loss as:

$$L_r = \sum_{t=1}^{T} \log \pi(A_t \mid S_t) R_t, \tag{7}$$

where $R_t = \sum_{k=0}^{T-t} \gamma^k r_{t+k}$ denotes a discounted accumulated reward, $\pi \sim \mathcal{N}(\mu_t, 1)$. The total loss is defined as:

$$L_{total} = L_c + \rho L_r, \tag{8}$$

where ρ is a scalar hyper-parameter. The pseudocode of our approach is described in Algorithm 1.

Table 1: Few-shot *5-way* classification accuracy and 95% confidence interval on *Mini*ImageNet dataset.

Model	Backbone	**1-shot**	**5-shot**
ProtoNet[44]	Conv-4	52.61±0.20	71.33±0.16
TEAM[36]	Conv-4	56.57	72.04
EPNet[41]	Conv-4	59.32±0.88	72.95±0.64
Curvature+T[13]	Conv-4	58.29±0.22	73.93±0.16
DSN-MR[42]	Conv-4	55.88±0.90	70.50±0.68
ALFA+MeTAL[5]	Conv-4	57.75±0.38	74.10±0.43
AIM[22]	Conv-4	61.90±0.57	74.55±0.38
RMO-PN	Conv-4	61.50±0.20	75.11±0.16
RMO-MON	Conv-4	60.15±0.20	74.64±0.18
RMO-DSN	Conv-4	**62.52±0.20**	**76.32±0.16**
ProtoNet[44]	ResNet-12	62.39±0.21	80.53±0.14
MetaOptNet[23]	ResNet-12	62.64±0.61	78.63±0.46
DSN-MR[42]	ResNet-12	64.60±0.72	79.51±0.50
CAN+T[18]	ResNet-12	67.19±0.55	80.64±0.35
Curvature+T[13]	ResNet-12	71.79±0.23	83.00±0.17
ALFA+MeTAL[5]	ResNet-12	66.61±0.28	84.40±0.44
LR+ICI[50]	ResNet-12	66.80	79.26
EPNet[41]	ResNet-12	66.50±0.89	81.06±0.60
RMO-PN	ResNet-12	71.21±0.20	86.03±0.15
RMO-MON	ResNet-12	69.71±0.22	85.52±0.15
RMO-DSN	ResNet-12	**73.74±0.20**	**86.69±0.15**
TEAM[36]	ResNet-18	60.07	75.90
TIM-GD[7]	ResNet-18	73.9	85.0
LaplacianShot[61]	ResNet-18	72.11±0.19	82.31±0.14
Oblique+T[35]	ResNet-18	77.20±0.36	87.11±0.42
RMO-PN	ResNet-18	75.31±0.20	86.32±0.15
RMO-DSN	ResNet-18	**77.85±0.20**	**87.54±0.16**
BD-CSPN[26]	WRN-28-10	70.31±0.93	81.89±0.60
AIM[22]	WRN-28-10	71.22±0.57	82.25±0.34
LaplacianShot[61]	WRN-28-10	74.86±0.19	84.13±0.14
EPNet[41]	WRN-28-10	70.74±0.85	84.34±0.53
TIM-GD[7]	WRN-28-10	77.8	87.4
Oblique+T[35]	WRN-28-10	80.64±0.34	89.39±0.39
RMO-PN	WRN-28-10	79.27±0.19	87.81±0.16
RMO-DSN	WRN-28-10	**81.08±0.20**	**89.97±0.16**

Table 2: Few-shot *5-way* classification accuracy and 95% confidence interval on *Tiered*ImageNet dataset.

Model	Backbone	**1-Shot**	**5-Shot**
ProtoNet[44]	Conv4	52.28±0.21	71.34±0.18
TPN[27]	Conv-4	59.91±0.94	73.30±0.75
EPNet[41]	Conv-4	59.97±0.95	73.91±0.75
ALFA+MeTAL[5]	Conv-4	60.29±0.37	75.88±0.29
RMO-PN	Conv-4	62.10±0.20	77.80±0.19
RMO-MON	Conv-4	61.82±0.21	76.24±0.19
RMO-DSN	Conv-4	**63.39±0.20**	**78.84±0.18**
ProtoNet[44]	ResNet-12	68.23±0.23	84.03±0.16
MetaOptNet[23]	ResNet-12	65.99±0.72	81.56±0.53
DSN-MR[42]	ResNet-12	67.39±0.82	82.85±0.56
CAN+T[18]	ResNet-12	73.21±0.58	84.93±0.38
Curvature+T[13]	ResNet-12	77.19±0.24	86.18±0.15
ALFA+MeTAL[5]	ResNet-12	70.29±0.40	86.17±0.35
EPNet[41]	ResNet-12	76.53±0.87	87.32±0.64
LR+ICI[50]	ResNet-12	80.79	87.92
RMO-PN	ResNet-12	80.29±0.23	87.54±0.16
RMO-MON	ResNet-12	79.44±0.25	87.09±0.19
RMO-DSN	ResNet-12	**81.11±0.23**	**88.22±0.16**
TIM-GD[7]	ResNet-18	79.9	88.5
LaplacianShot[61]	ResNet-18	78.98±0.21	86.39±0.16
Oblique+T[35]	ResNet-18	83.73±0.36	90.46±0.46
RMO-PN	ResNet-18	82.05±0.23	88.67±0.16
RMO-DSN	ResNet-18	**84.03±0.23**	**90.86±0.16**
BD-CSPN[26]	WRN-28-10	78.74±0.95	86.92±0.63
LaplacianShot[61]	WRN-28-10	80.18±0.21	87.56±0.15
EPNet[41]	WRN-28-10	78.50±0.91	88.36±0.57
TIM-GD[7]	WRN-28-10	82.1	89.8
Oblique+T[35]	WRN-28-10	85.22±0.34	91.35±0.42
RMO-PN	WRN-28-10	83.66±0.22	89.23±0.18
RMO-DSN	WRN-28-10	**85.54±0.22**	**91.72±0.18**

4 EXPERIMENTS

4.1 Datasets

We evaluate our approach on 3 benchmark datasets: *Mini*ImageNet [47], *Tiered*ImageNet [38], and CUB-200-2011 [48]. *Mini*ImageNet and *Tiered*ImageNet are two subsets of ImageNet [11] dataset. *Mini*ImageNet dataset contains 100 categories with 600 images per category. Following the splits provided by Ravi *et al.* [37], we split the 100 categories into 64, 16, and 20 categories for training, validation, and evaluation, respectively. *Tiered*ImageNet is a large-scale dataset containing 351, 97, and 160 categories for training, validation, and evaluation, respectively. The CUB-200-2011 dataset contains 200 categories with a total number of 11788 images. Following the protocol of Hilliard *et al.* [16], we split the dataset into 100, 50, and 50 categories for training, validation, and evaluation, respectively.

4.2 Implementation Details

We utilize 4 commonly used backbones in few-shot learning: Conv-4 [21], ResNet-12 [15], ResNet-18 [15], and WRN-28-10 [58]. The backbone takes a 3×84×84 image as input. For Conv-4, the Adam optimizer is utilized. For ResNets and WRN, the SGD optimizer is utilized with momentum of 0.9 and weight decay of 0.0005. We insert a FiLM layer after the last BN layer in the convolution blocks of the backbone. The parameters γ_t and β_t of each FiLM layer are concatenated to form the action A_t. The value of T, D, and γ is set

Table 3: Few-shot *5-way* classification accuracy and 95% confidence interval on the CUB-200-2011 dataset.

Model	Backbone	**1-Shot**	**5-Shot**
ProtoNet[44]	Conv-4	63.72±0.22	81.50±0.15
EPNet[41]	Conv-4	65.94±0.93	78.80±0.64
TEAM[36]	Conv-4	75.71	86.04
BD-CSPN[26]	Conv-4	75.10	87.25
Curvature+T[13]	Conv-4	76.69±0.21	**89.30±0.12**
RMO-PN	Conv-4	75.96±0.23	87.56±0.15
RMO-MON	Conv-4	74.28±0.25	85.54±0.17
RMO-DSN	Conv-4	**77.26±0.24**	88.73±0.16
ProtoNet[44]	ResNet-12	66.09±0.92	82.50±0.58
BD-CSPN[26]	ResNet-12	84.90	90.22
EPNet[41]	ResNet-12	82.85±0.81	91.32±0.41
LR+ICI[50]	ResNet-12	**88.06**	92.53
RMO-PN	ResNet-12	84.60±0.21	91.39±0.12
RMO-MON	ResNet-12	83.32±0.26	90.31±0.18
RMO-DSN	ResNet-12	86.79±0.21	**92.82±0.13**
ProtoNet[44]	ResNet-18	72.99±0.88	86.65±0.51
TEAM[36]	ResNet-18	80.16	87.17
TIM-GD[7]	ResNet-18	82.2	90.8
LaplacianShot[61]	ResNet-18	80.96	88.68
Oblique+T[35]	ResNet-18	85.87	94.97
RMO-PN	ResNet-18	86.46±0.23	93.69±0.14
RMO-DSN	ResNet-18	**87.57±0.23**	**95.16±0.14**
BD-CSPN[26]	WRN-28-10	87.45	91.74
EPNet[41]	WRN-28-10	87.75±0.70	94.03±0.33
RMO-PN	WRN-28-10	86.76±0.22	93.67±0.13
RMO-DSN	WRN-28-10	**88.56±0.22**	**95.27±0.13**

Table 4: Few-shot *5-way* classification accuracy and 95% confidence interval with DenseNet backbone.

Method	*Mini*ImageNet		*Tiered*ImageNet	
	1-shot	5-shot	1-shot	5-shot
SimpleShot[49]	65.77±0.19	82.23±0.13	71.20±0.22	86.33±0.15
LaplacianShot[61]	75.57±0.19	84.72±0.13	80.30±0.20	87.93±0.15
RAP-LaplacianShot[17]	75.58±0.20	85.63±0.13	-	-
ICA+MSP[25]	77.06±0.26	84.99±0.14	84.29±0.25	89.31±0.15
RMO-PN	78.26±0.19	84.92±0.14	85.15±0.21	89.25±0.15
RMO-DSN	**79.83±0.19**	**86.47±0.13**	**86.09±0.20**	**91.16±0.15**

to 5, 2000, and 0.9, respectively. The value of ρ is set to $\frac{2}{\sum_{i=1}^{T} i}$. First, we pre-train the backbone following the settings of the prior work [55]. Then, the whole model is meta-trained for 200 epochs, with each epoch including 100 randomly sampled tasks. We scale the learning rate of weights of the backbone by 0.1 in meta-training. In validation, we use 600 randomly sampled tasks to choose the best model. During evaluation, we report the classification accuracy and 95% interval confidence over 10000 randomly sampled tasks. Each task includes 15 query samples per class in all settings. We take the averaged results using 3 different random seeds. The learning rate is set to 0.002 and 0.001 for ConvNet and three ResNets, respectively. We scale the initial learning rate by 0.2 after every 30 epochs in meta-training. Our code is based on PyTorch [31], and all experiments are conducted using an NVIDIA RTX A6000 GPU. More details are provided in **Supplementary Material**.

Table 5: Few-shot *5-way* classification accuracy comparing to CNAPS and Simple-CNAPS. "In." denotes "inductive".

Method	*Mini*ImageNet		*Tiered*ImageNet	
	1-shot	5-shot	1-shot	5-shot
CNAPS[39]	77.99	87.31	75.12	86.57
Simple-CNAPS[6]	82.16	89.80	78.29	89.01
RMO-PN (In.)	80.93	89.21	77.75	89.25
RMO-DSN (In.)	**83.12**	**90.76**	**79.35**	**90.16**

4.3 Main Results

Table 1, Table 2, and Table 3 list the results of our method on *Mini*ImageNet, *Tiered*ImageNet, and CUB-200-2011, respectively. We mainly compare our approach with the previous state-of-the-art transductive few-shot learning approaches, including Curvature [13], TEAM [36], Oblique [35], EPNet [41], TIM [7], ICI [50], LaplacianShot [61], and BD-CSPN [26]. It can be seen that our approach shows consistent improvements over other transductive few-shot learning approaches on all three datasets using the four backbones. For example, under 1-shot and 5-shot on *Mini*ImageNet with ResNet-12, our approach shows on average +2.3%, +5.8%, and +4.2% performance gains comparing to Curvature [13], CAN [18], and MeTAL [5], respectively. On *Tiered*ImageNet with ResNet-12, our approach shows on average +3.0%, +5.6%, and +6.4% performance gains comparing to the above three methods. On CUB-200-2011, our approach also shows on average +2.9% and +4.8% performance gains with TIM [7] and EPNet [41], respectively. The promising results suggest that our approach makes it easier to reach a better local optima on the loss surface of the meta-training phase via exploring stable meta-optimization patterns, thus improving the discriminative ability of global embeddings.

4.4 Ablation Study

In this section, we first explore hyper-parameters' impacts on the proposed strategy. Then, we analyze the impacts of different modules on classification performance. Besides, we extend our strategy to the DenseNet backbone. Furthermore, we conduct experiments on the challenging cross-domain and generalized few-shot tasks. For simplicity, "PN", "DSN", and "MON" denote RMO-PN, RMO-DSN, and RMO-MON, respectively.

Selection of hyper-parameters. We describe how we choose the value of hyper-parameter T, D, and γ in **Supplementary Material**.

Impacts of different modules. We analyze the impact of each module, *i.e.*, policy, memory, and task state encoder (denoted as "GRU", "DND", and "SATT", respectively). The experiments are conducted under 5-shot 5-way on *Mini*ImageNet. Relative results are listed in Table 6. To show the effects of differentiable RL and memory mechanism, we replace GRU and DND with two FC layers

Table 6: Classification accuracy and 95% confidence interval on different combinations of the modules in our approach.

Settings	SATT	GRU	DND	Conv-4			ResNet-12			ResNet-18	
				PN	DSN	MON	PN	DSN	MON	PN	DSN
	✓			72.33±0.16	73.29±0.18	71.27±0.17	82.76±0.14	83.16±0.18	82.19±0.18	84.74±0.15	84.66±0.15
		✓		73.18±0.16	73.60±0.17	72.21±0.17	83.17±0.15	83.72±0.19	83.30±0.17	84.39±0.15	85.30±0.15
		✓	✓	73.86±0.16	74.42±0.17	73.03±0.17	83.91±0.15	84.63±0.20	84.21±0.17	84.91±0.15	85.86±0.15
	✓	✓		74.61±0.16	75.64±0.17	73.81±0.17	85.37±0.15	85.86±0.19	84.97±0.17	85.65±0.15	86.73±0.15
	✓	✓	✓	75.11±0.16	76.32±0.16	74.64±0.18	86.03±0.15	86.69±0.15	85.52±0.15	86.32±0.15	87.54±0.16

Table 7: Few-shot *5-way* classification accuracy and 95% confidence interval on cross-domain task: *Mini*ImageNet → CUB-200-2011 dataset.

Setups	Backbone	**1-Shot**	**5-Shot**
ProtoNet[44]	ResNet-18	-	62.02±0.70
SimpleShot[49]	ResNet-18	48.56	65.63
MetaOptNet[23]	ResNet-12	44.79±0.75	64.98±0.68
LaplacianShot[61]	ResNet-18	55.46	66.33
ALFA+MeTAL[5]	ResNet-12	-	70.22±0.14
Centroid[2]	ResNet-18	46.85±0.75	70.37±1.02
TIM-GD[7]	ResNet-18	-	71.0
Oblique+T[35]	ResNet-18	-	74.11
RMO-PN	ResNet-18	54.67±0.18	73.58±0.18
RMO-DSN	ResNet-18	**56.82±0.18**	**74.64±0.16**

Table 8: Classification accuracy and 95% confidence interval on generalized few-shot task. "In." denotes "inductive".

Setup	Model	**SEEN**	**UNSEEN**	**COMBINED**
1-shot	ProtoNet[44]	41.73±0.03	48.64±0.20	35.69 ±0.03
	FEAT[55]	43.94±0.03	49.72±0.20	40.50 ±0.03
	RMO-PN (In.)	48.00±0.04	53.68±0.19	43.61 ±0.04
	RMO-MON (In.)	46.96±0.04	52.21±0.19	42.80 ±0.03
	RMO-DSN (In.)	**49.34±0.04**	**54.16±0.19**	**44.02 ±0.03**
5-shot	ProtoNet[44]	41.06±0.03	64.94±0.17	38.04 ±0.02
	FEAT[55]	44.94±0.03	65.33±0.16	41.68 ±0.03
	RMO-PN (In.)	49.56±0.03	68.37±0.19	44.52 ±0.05
	RMO-MON (In.)	48.71±0.03	67.54±0.18	43.50 ±0.04
	RMO-DSN (In.)	**50.40±0.03**	**69.02±0.17**	**45.13 ±0.04**

to learn the parameters γ and β. To show the effects of information adaptation from query set when constructing task state, we replace SATT with an averaging operation, *i.e.*, obtaining the task state via averaging the mean vectors represented by each class as Oreshkin *et al.* [30]. It can be observed that the differentiable RL strategy and memory mechanism bring about +3% performance improvement, comparing to learning FiLM layer parameters with FC layers. Besides, the information adaptation from query set also shows about +2% performance improvement.

Table 9: Time complexity of the three models.

Models	Classifier	Total
RMO-PN	$O(NKd)$	$O(T(NK)^2d)$
RMO-DSN	$O(NKd^2)$	$O(max(TNKd^2, T(NK)^2d))$
RMO-MON	$O(d^3)$	$O(Td^3)$

Table 10: Standard deviations of the loss function.

Setting →	5-way 1-shot					
Backbone	PN	DSN	MON	RMO-PN	RMO-DSN	RMO-MON
Conv-4	0.266	0.308	0.251	**0.128**	0.165	0.191
ResNet-12	0.108	0.101	0.178	0.036	**0.016**	0.053
ResNet-18	0.127	0.102	0.201	0.042	**0.015**	0.041
Setting →	5-way 5-shot					
Backbone	PN	DSN	MON	RMO-PN	RMO-DSN	RMO-MON
Conv-4	0.382	0.405	0.252	**0.158**	0.168	0.183
ResNet-12	0.059	0.085	0.108	0.037	**0.016**	0.052
ResNet-18	0.054	0.035	0.067	0.034	**0.013**	0.041

Time complexity. The time complexity in each time step for SATT, GRU, and DND are $O((NK)^2d)$, $O(d^2)$, and $O(Dd)$, respectively. The total time complexities of the three models are listed in Table 9. Here we assume $d^3 \gg (NK)^2 \gg D \gg d$.

Standard deviation of loss function. The standard deviation of the loss function can verify the stabilizing effects of our approach. We calculate the standard deviation of the loss function in the last 100 epochs. The experiments are conducted under 5-way 5-shot and 5-way 1-shot on *Mini*ImageNet. Table 10 lists the results. It can be seen that our three models achieve lower standard deviations comparing to the three baseline models [23, 42, 44].

DenseNet backbone performance. Following the settings of Lichtenstein *et al.* [25], we measure the performance of our approach with DenseNet [19] backbone. Specifically, we insert a FiLM layer after the last BN layer in each dense block of DenseNet-121. The backbone is first pre-trained following the protocol of prior work [49]. The experiments are conducted under 5-way 5-shot and 5-way 1-shot on *Mini*ImageNet and *Tiered*ImageNet. Relative results are listed in Table 4. Our approach outperforms previous state-of-the-art transductive methods by about +1.8%, including RAP-LaplacianShot [17] and TAFSSL [25]. This suggests our approach also contributes to dense connection-based backbones. More details are provided in **Supplementary Material**.

Comparisons with typical task-adaptive methods. We compare the few-shot classification performance of our approach with two

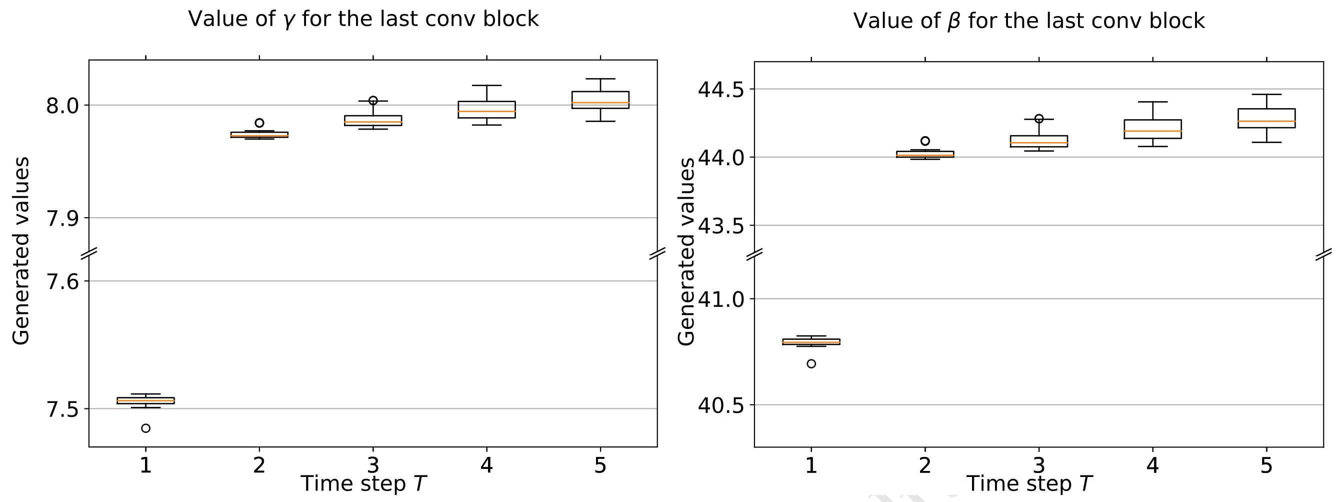

Figure 4: Visualization of the values of parameters γ and β. We depict the boxplots of γ and β respectively for the last convolution block of Conv-4 backbone before the last max-pooling layer.

typical state-of-the-art approaches using FiLM layers: CNAPS [39] and Simple-CNAPS [6]. For a fair comparison, we utilize ResNet-18 pre-trained on ImageNet as backbone, and we insert a FiLM layer after the last BN layer in each residual block of ResNet-18. The model is meta-trained following the settings in Simple-CNAPS [6]. Since the works [6, 39] are inductive methods, we utilize only the support samples when calculating the task state (*i.e.*, use all support samples as query instead of all query samples). Relative results are listed in Table 5. Our method outperforms Simple-CNAPS by about +1% on average on *Mini*ImageNet and *Tiered*ImageNet. This suggests our method also takes impacts with feature-rich backbones, comparing to directly learning parameters of FiLM layers. More details are provided in **Supplementary Material**.

Cross-domain few-shot classification performance. Following the splits introduced by Chen *et al.* [8], we meta-train the model on the entire *Mini*ImageNet dataset (*i.e.*, training set, validation set, and testing set), then meta-test the model on the test split of CUB-200-2011 dataset. Relative results are listed in Table 7. We show obvious improvements in our approach under both 1-shot and 5-shot settings compared to other state-of-the-art cross-domain methods. This suggests that the differentiable RL strategy contributes to improving the discriminative ability of task-specific embeddings even when a domain gap exists.

Generalized few-shot classification performance. Following the splits of Ye *et al.* [55], we first train the model only on seen classes $\mathbb{S}$ of *Mini*ImageNet dataset under 1-shot 5-way and 5-shot 5-way. Then we evaluate the model with three criteria: UNSEEN evaluates the 5-way classification accuracy only on unseen classes $\mathbb{U}$; SEEN evaluates the 64-way classification accuracy only on seen classes $\mathbb{S}$; COMBINED evaluates the 69-way mixed classification accuracy on both seen and unseen classes. We use the inductive versions of our method in the experiments. Relative results are listed in Table 8. Our method shows about +4.3% and +6.9% performance gains against FEAT [55] and ProtoNet [44] respectively on the 3 evaluation criteria. This suggests that our approach also contributes to not forgetting previously learned class knowledge.

Visualization. We depict the statistical distributions, represented as boxplots, of the parameters γ and β in each time step t across different meta-tasks in Figure 4. We visualize the parameters γ and β for the last convolution block of Conv-4 backbone. It can be observed that the parameters γ and β have larger influence on the embedding procedure with longer time steps. Further, it can be seen that the generated parameter values vary among different tasks to a larger extent when the time step goes longer, especially at the last time step T. This suggests that the model learns to adapt to each meta-task generally across time steps via differentiable RL. Besides, we plot the curves of validation accuracy on *Mini*ImageNet and *Tiered*ImageNet among our models and ProtoNet. The results are reported in **Supplementary Material**.

5 CONCLUSION

This work proposes a generic differentiable RL-based meta optimization strategy for few-shot learning, aiming to explore stable meta-optimization patterns in meta-training. Due to the differentiability of the environment, our approach can avoid the flaws of black-box RL. This approach is a new way of introducing RL strategy into few-shot learning. The approach contains a policy equipped with the memory for learning generalizable optimizations of embedding procedure across unseen tasks. In addition, we propose a task state encoder to adapt information from the query set to the support set for fully exploring inner-task similarities. Our strategy can be easily applied to various backbones, including ConvNet, ResNet, WRN, and DenseNet. Our method also shows promising results on the challenging cross-domain and generalized few-shot classification tasks. Lastly, this work shows the huge benefits of exploring stable patterns in meta-learning, however it has limitations on model complexity. Future work includes studying the model efficiency and applying this approach to multiple downstream tasks.

REFERENCES

[1] Arman Afrasiyabi, Jean-François Lalonde, and Christian Gagné. 2020. Associative alignment for few-shot image classification. In *ECCV*. 18–35.

[2] Arman Afrasiyabi, Jean-François Lalonde, and Christian Gagné. 2020. Associative alignment for few-shot image classification. In *ECCV*. 18–35.

[3] Raviteja Anantha, Stephen Pulman, and Srinivas Chappidi. 2020. Generalized Reinforcement Meta Learning for Few-Shot Optimization. In *ICML*.

[4] Antreas Antoniou, Harrison Edwards, and Amos J. Storkey. 2019. How to train your MAML. In *ICLR*.

[5] Sungyong Baik, Janghoon Choi, Heewon Kim, Dohee Cho, Jaesik Min, and Kyoung Mu Lee. 2021. Meta-Learning with Task-Adaptive Loss Function for Few-Shot Learning. In *ICCV*. 9465–9474.

[6] Peyman Bateni, Raghav Goyal, Vaden Masrani, Frank Wood, and Leonid Sigal. 2020. Improved few-shot visual classification. In *CVPR*. 14493–14502.

[7] M Boudiaf, ZI Masud, J Rony, J Dolz, P Piantanida, and IB Ayed. 2020. Transductive information maximization for few-shot learning. In *NeurIPS*.

[8] Wei-Yu Chen, Yen-Cheng Liu, Zsolt Kira, Yu-Chiang Wang, and Jia-Bin Huang. 2019. A Closer Look at Few-shot Classification. In *ICLR*.

[9] Wen-Hsuan Chu, Yu-Jhe Li, Jing-Cheng Chang, and Yu-Chiang Frank Wang. 2019. Spot and learn: A maximum-entropy patch sampler for few-shot image classification. In *CVPR*. 6251–6260.

[10] Filipe de Avila Belbute-Peres, Kevin Smith, Kelsey Allen, Josh Tenenbaum, and J Zico Kolter. 2018. End-to-end differentiable physics for learning and control. In *NeurIPS*, Vol. 31.

[11] Jia Deng, Wei Dong, Richard Socher, Li-Jia Li, Kai Li, and Li Fei-Fei. 2009. Imagenet: A large-scale hierarchical image database. In *CVPR*. 248–255.

[12] Chelsea Finn, Pieter Abbeel, and Sergey Levine. 2017. Model-agnostic meta-learning for fast adaptation of deep networks. In *ICML*. 1126–1135.

[13] Zhi Gao, Yuwei Wu, Yunde Jia, and Mehrtash Harandi. 2021. Curvature generation in curved spaces for few-shot learning. In *ICCV*. 8691–8700.

[14] Danijar Hafner, Timothy Lillicrap, Jimmy Ba, and Mohammad Norouzi. 2020. Dream to control: Learning behaviors by latent imagination. In *ICLR*.

[15] Kaiming He, Xiangyu Zhang, Shaoqing Ren, and Jian Sun. 2016. Deep residual learning for image recognition. In *CVPR*. 770–778.

[16] Nathan Hilliard, Lawrence Phillips, Scott Howland, Artëm Yankov, Courtney D Corley, and Nathan O Hodas. 2018. Few-shot learning with metric-agnostic conditional embeddings. (2018). arXiv preprint arXiv:1802.04376.

[17] Jie Hong, Pengfei Fang, Weihao Li, Tong Zhang, Christian Simon, Mehrtash Harandi, and Lars Petersson. 2021. Reinforced attention for few-shot learning and beyond. In *CVPR*. 913–923.

[18] Ruibing Hou, Hong Chang, Bingpeng Ma, Shiguang Shan, and Xilin Chen. 2019. Cross attention network for few-shot classification. In *NeurIPS*, Vol. 32.

[19] Gao Huang, Zhuang Liu, Laurens Van Der Maaten, and Kilian Q Weinberger. 2017. Densely connected convolutional networks. In *CVPR*. 4700–4708.

[20] Dahyun Kang, Heeseung Kwon, Juhong Min, and Minsu Cho. 2021. Relational embedding for few-shot classification. In *ICCV*. 8822–8833.

[21] Alex Krizhevsky, Ilya Sutskever, and Geoffrey E Hinton. 2012. ImageNet Classification with Deep Convolutional Neural Networks. In *NeurIPS*, Vol. 25.

[22] Eugene Lee, Cheng-Han Huang, and Chen-Yi Lee. 2021. Few-shot and continual learning with attentive independent mechanisms. In *ICCV*. 9455–9464.

[23] Kwonjoon Lee, Subhransu Maji, Avinash Ravichandran, and Stefano Soatto. 2019. Meta-learning with differentiable convex optimization. In *CVPR*. 10657–10665.

[24] Hongyang Li, David Eigen, Samuel Dodge, Matthew Zeiler, and Xiaogang Wang. 2019. Finding task-relevant features for few-shot learning by category traversal. In *CVPR*. 1–10.

[25] Moshe Lichtenstein, Prasanna Sattigeri, Rogerio Feris, Raja Giryes, and Leonid Karlinsky. 2020. TAFSSL: Task-adaptive feature sub-space learning for few-shot classification. In *ECCV*. 522–539.

[26] Jinlu Liu, Liang Song, and Yongqiang Qin. 2020. Prototype rectification for few-shot learning. In *ECCV*. 741–756.

[27] Yanbin Liu, Juho Lee, Minseop Park, Saehoon Kim, Eunho Yang, Sung Ju Hwang, and Yi Yang. 2019. Learning to propagate labels: Transductive propagation network for few-shot learning. In *ICLR*.

[28] Yang Liu, Weifeng Zhang, Chao Xiang, Tu Zheng, Deng Cai, and Xiaofei He. 2022. Learning to affiliate: Mutual centralized learning for few-shot classification. In *CVPR*. 14411–14420.

[29] Michael Lutter, Johannes Silberbauer, Joe Watson, and Jan Peters. 2021. Differentiable physics models for real-world offline model-based reinforcement learning. In *ICRA*. 4163–4170.

[30] Boris Oreshkin, Pau Rodríguez López, and Alexandre Lacoste. 2018. Tadam: Task dependent adaptive metric for improved few-shot learning. In *NeurIPS*, Vol. 31.

[31] Adam Paszke, Sam Gross, et al. 2019. Pytorch: An imperative style, high-performance deep learning library. In *NeurIPS*, Vol. 32. 8026–8037.

[32] Zhimao Peng, Zechao Li, Junge Zhang, Yan Li, Guo-Jun Qi, and Jinhui Tang. 2019. Few-shot image recognition with knowledge transfer. In *ICCV*. 441–449.

[33] Ethan Perez, Florian Strub, Harm De Vries, Vincent Dumoulin, and Aaron Courville. 2018. Film: Visual reasoning with a general conditioning layer. In *AAAI*, Vol. 32.

[34] Alexander Pritzel, Benigno Uria, Sriram Srinivasan, Adria Puigdomenech Badia, Oriol Vinyals, Demis Hassabis, Daan Wierstra, and Charles Blundell. 2017. Neural episodic control. In *ICML*. 2827–2836.

[35] Guodong Qi, Huimin Yu, Zhaohui Lu, and Shuzhao Li. 2021. Transductive few-shot classification on the oblique manifold. In *ICCV*. 8412–8422.

[36] Limeng Qiao, Yemin Shi, Jia Li, Yaowei Wang, Tiejun Huang, and Yonghong Tian. 2019. Transductive episodic-wise adaptive metric for few-shot learning. In *ICCV*. 3603–3612.

[37] Sachin Ravi and Hugo Larochelle. 2017. Optimization as a model for few-shot learning. In *ICLR*.

[38] Mengye Ren, Eleni Triantafillou, Sachin Ravi, Jake Snell, Kevin Swersky, Joshua B. Tenenbaum, Hugo Larochelle, and Richard S. Zemel. 2018. Meta-Learning for Semi-Supervised Few-Shot Classification. In *ICLR*.

[39] James Requeima, Jonathan Gordon, John Bronskill, Sebastian Nowozin, and Richard E Turner. 2019. Fast and flexible multi-task classification using conditional neural adaptive processes. In *NeurIPS*, Vol. 32.

[40] Samuel Ritter, Jane Wang, Zeb Kurth-Nelson, Siddhant Jayakumar, Charles Blundell, Razvan Pascanu, and Matthew Botvinick. 2018. Been there, done that: Meta-learning with episodic recall. In *ICML*. 4354–4363.

[41] Pau Rodríguez, Issam Laradji, Alexandre Drouin, and Alexandre Lacoste. 2020. Embedding propagation: Smoother manifold for few-shot classification. In *ECCV*. 121–138.

[42] Christian Simon, Piotr Koniusz, Richard Nock, and Mehrtash Harandi. 2020. Adaptive subspaces for few-shot learning. In *CVPR*. 4136–4145.

[43] Christian Simon, Piotr Koniusz, Richard Nock, and Mehrtash Harandi. 2020. On modulating the gradient for meta-learning. In *ECCV*. 556–572.

[44] Jake Snell, Kevin Swersky, and Richard Zemel. 2017. Prototypical networks for few-shot learning. In *NeurIPS*, Vol. 30.

[45] Nitish Srivastava, Geoffrey Hinton, Alex Krizhevsky, Ilya Sutskever, and Ruslan Salakhutdinov. 2014. Dropout: a simple way to prevent neural networks from overfitting. *Journal of machine learning research* 15, 1 (2014), 1929–1958.

[46] Hung-Yu Tseng, Hsin-Ying Lee, Jia-Bin Huang, and Ming-Hsuan Yang. 2020. Cross-domain few-shot classification via learned feature-wise transformation. In *ICLR*.

[47] Oriol Vinyals, Charles Blundell, Timothy Lillicrap, Daan Wierstra, et al. 2016. Matching networks for one shot learning. In *NeurIPS*, Vol. 29.

[48] C. Wah, S. Branson, P. Welinder, P. Perona, and S. Belongie. 2011. *The caltech-ucsd birds-200-2011 dataset*. Technical Report CNS-TR-2011-001. California Institute of Technology.

[49] Yan Wang, Wei-Lun Chao, Kilian Q Weinberger, and Laurens van der Maaten. 2019. Simpleshot: Revisiting nearest-neighbor classification for few-shot learning. (2019). arXiv preprint arXiv:1911.04623.

[50] Yikai Wang, Chengming Xu, Chen Liu, Li Zhang, and Yanwei Fu. 2020. Instance credibility inference for few-shot learning. In *CVPR*. 12836–12845.

[51] Chen Xing, Negar Rostamzadeh, Boris Oreshkin, and Pedro Pinheiro. 2019. Adaptive cross-modal few-shot learning. In *NeurIPS*, Vol. 32.

[52] Jingjing Xu, Xu Sun, Zhiyuan Zhang, Guangxiang Zhao, and Junyang Lin. 2019. Understanding and improving layer normalization. In *NeurIPS*, Vol. 32.

[53] Ling Yang, Liangliang Li, Zilun Zhang, Xinyu Zhou, Erjin Zhou, and Yu Liu. 2020. Dpgn: Distribution propagation graph network for few-shot learning. In *CVPR*. 13390–13399.

[54] Han-Jia Ye and Wei-Lun Chao. 2022. How to train your MAML to excel in few-shot classification. In *ICLR*.

[55] Han-Jia Ye, Hexiang Hu, De-Chuan Zhan, and Fei Sha. 2020. Few-shot learning via embedding adaptation with set-to-set functions. In *CVPR*. 8808–8817.

[56] Mingzhang Yin, George Tucker, Mingyuan Zhou, Sergey Levine, and Chelsea Finn. 2020. Meta-learning without memorization. In *ICLR*.

[57] Sung Whan Yoon, Jun Seo, and Jaekyun Moon. 2019. Tapnet: Neural network augmented with task-adaptive projection for few-shot learning. In *ICML*. 7115–7123.

[58] Sergey Zagoruyko and Nikos Komodakis. 2016. Wide Residual Networks. In *BMVC*.

[59] Chi Zhang, Yujun Cai, Guosheng Lin, and Chunhua Shen. 2020. Deepemd: Few-shot image classification with differentiable earth mover's distance and structured classifiers. In *CVPR*. 12203–12213.

[60] Guo-Bing Zhou, Jianxin Wu, Chen-Lin Zhang, and Zhi-Hua Zhou. 2016. Minimal gated unit for recurrent neural networks. *International Journal of Automation and Computing* 13, 3 (2016), 226–234.

[61] Imtiaz Ziko, Jose Dolz, Eric Granger, and Ismail Ben Ayed. 2020. Laplacian regularized few-shot learning. In *ICML*. 11660–11670.